

Populärvetenskaplig sammanfattning

Glaukom (vanligen benämnd som grön starr) är en global folksjukdom som även med behandling kan leda till blindhet. Vid glaukom uppstår skadorna i samband med ökat tryck i ögat.

Synnerven leder information från ögat till hjärnan via synnerven - en hopsamling nervfibrer med bas i näthinnan. Sjukdomsmekanismen vid glaukom skadar dessa nervfibrer, vilket gör att de så småningom dör. Förlusten av nervfibrerna är kontinuerlig över tid, vilket kan skattas som en uttunning av nervfibrerna kring papillen. Tjockleken av nervfiberlagret blir konstaterat mindre kring synnervshuvudet.

Det första symtomet är vanligen perifert synfältsbortfall. Vid det laget har irreversibla skador i nerfiberlagret redan uppstått och den enda behandling som finns framöver syftar till att stävja vidare progress av sjukdomen genom att sänka ögontrycket.

Det har gjorts flera studier som handlat om hur nervfiberlagret bäst ska avbildas och mätas. Optisk koherenstomografi (förkortat OCT, Optical Coherence Tomography) är en icke-invasiv och objektiv metod att visualisera strukturer i ögat, däribland synnervspapillen. Genom att definiera mått för nerfiberlagrets tjocklek kring synnervshuvudet öppnas möjligheten att i spåra dess ändringar i syfte att tidigare upptäcka glaukom och progress av sjukdomen.

Tre olika parametrar för mätning med OCT har föreslagits. Denna studie använder sig av en relativt ny parameter för tjockleken av nervfiberlagret runt synnervshuvudet: PIMD. Medelvärde av detta mått är $PIMD-2\pi$. Genom att mäta PIMD i 500 projektioner runt synnervshuvudet och beräkna genomsnittet av dessa, fås ett medelvärde av tjockleken hos en individ. Detta värde har i tidigare studier visat sig vara rätt konstant och unikt för varje individ.

Denna studie undersökte hur medelvärdet förändras i olika grupper med ett åldersspann på 30-69 år. Det genomsnittliga $PIMD-2\pi$ värdet i varje åldersgrupp togs fram och analyserades statistiskt. Resultatet visade inte på några betydande skillnader av genomsnittligt $PIMD-2\pi$ mellan åldersgrupperna. Däremot sågs en trend med en liten förlust av vävnad per år hos friska ögon.

Resultatet ska tolkas med osäkerhet eftersom stickprovet var för litet. Den automatiska algoritmen producerade resultat som stämmer överens med en semi-automatisk metod för PIMD-mätning samt för tidigare forskningsresultat där andra parametrar använts.

I framtiden behöver större stickprov tas för att kunna dra slutsatser om åldersrelaterad normalförlust av nervfibrerna. Kunskapen kan användas för att definiera och särskilja normal och patologisk förlust med stigande ålder.

Abstract

Background: Glaucoma is a progressive which leads to vision loss due to damage of the RGC axons. Optical coherence tomography (OCT) is a clinical staple tool which can used to objectively measure the cross-sectional content of RGC axons in the optic disc. PIMD is a proposed measurement parameter, averaged over the circumference of the optic disc (PIMD- 2π).

Purpose: to investigate differences in mean PIMD- 2π in non-glaucomatous samples in the ages 30-69 with the help of an automatical algorithm for measurement of PIMD.

Method: Three left-eye samples from 16 non-glaucomatous subjects equally balanced in age groups yielded 48 samples in total. The samples were averaged for each subject. A total of 16 PIMD- 2π measurements were investigated with ANOVA for variation sources and potential trends with a linear regression model.

Results: There was no statistical difference in mean PIMD- 2π in different age groups. The linear regression equation presented with a slope coefficient corresponding to a loss rate of $-2.43 \mu\text{m}/\text{year}$.

Conclusions: A sample size of 16 is too small to draw any conclusions about non-glaucomatous age-related loss of RGC axons in the ONH, but the results were similar previous studies with PIMD- 2π and other parameters. The automatic algorithm accurately segmented PIMD. For diagnostic purpose, longitudinal studies with larger healthy sample sizes need to be obtained to draw conclusions on non-glaucomatous age-related RGC axon loss in the ONH.

Background

Anatomy of the optic nerve head

The optic nerve head (ONH), or optic disc, is comprised of several different tissue structures located at the point where all the retinal nerve cell axons turn to exit the eye as the optic nerve (Appendix 1). Herein included are also major blood vessels such as the retinal artery and vein. In the ONH, the inner border is the vitreoretinal interface. It consists of the innermost retinal layer, the internal limiting membrane (ILM), which is connected to the vitreous cortex. The outer border of the ONH is Bruch's membrane, which consists of five sublayers; the topmost is the basement membrane of the retinal pigmental epithelium (RPE). The RPE is the outermost part of the retinal nerve fiber layer (RNFL) which contains the retinal ganglion cell (RGC) axons.

Outside of the ONH the RNFL runs adjacent to the vitreous body until making a perpendicular turn at the optic cup. The structure between the optic cup and ONH is the neuroretinal rim. In this area,

RGC axons can't penetrate the basement membrane of the retinal pigmental epithelium; thus, the entirety of them must pass between the central limit of the pigmental epithelium and the vitreoretinal interface. The RNFL with its RGC axons thickens considerably in the superior and inferior poles of the ONH border¹. The size and thickness of the ONH varies greatly among individuals, as well as the angle of insertion for the optic nerve².

The cup itself contains no RGC axons from the RNFL. Below the cup and the outermost retinal layer, formed by retinal pigment epithelium (RPE) attached to the choroid, axons continue to rearrange through the netlike *lamina cribrosa* in papillomaculary bundles, forming the complete structure of the exiting optic nerve.

Glaucoma

Glaucoma represents a collection of conditions with various pathophysiology that results in increased intraocular pressure (IOP) and subsequent damage to the optic disc.

In primary glaucoma the flow of aqueous humour is disturbed; the open-angle variant is most common and is caused when drainage of aqueous humour through the trabecular meshwork is too slow.

Primary open-angle glaucoma (OAG) is a chronic and constantly progressive disease, and the second leading cause of blindness worldwide³. Very few have symptoms during the early stages; more than half of individuals diagnosed with glaucoma are initially unaware of symptoms and are discovered during routine controls in which an elevated IOP is found⁴. A peripheral vision acuity loss is the most common first symptom; at that point there is already a preceding structural damage to the NFL in the ONH. Although there are several theories on the pathogenesis⁵⁻⁷, RGC axons are believed to undergo apoptosis⁸. The loss manifests as a thinning of RNFL, which shifts the size proportion between the optic cup and neuroretinal rim. The size ratio between cup and optic disc (C/D) is frequently assessed in glaucoma diagnostics. There is a report on associated nerve tissue loss visible as early as six years prior to a pathological visual field test result⁹.

Damage to the RNFL in the ONH is permanent and irreversible; patients with primary open-angle glaucoma need frequent follow-ups and treatment to prevent further loss of vision.

The only treatment is to lower IOP and monitor further changes. The goal is to maintain as much sight as possible. Patients with confirmed elevated IOP, glaucomatous optic nerve damage and visual field loss, have a 22% risk for bilateral blindness over 20 years¹⁰.

As of present, there is no true gold standard method for diagnostics and follow-up of glaucoma. The diagnostic process thus relies on combining gonioscopy of the anterior chamber, ophthalmoscopic assessment of the optic disc appearance, testing the visual field, and IOP measurements. The latter is considered a risk factor, but 46% of patients suspected to have glaucoma will not show an increase in IOP on a routine visit to the clinic¹¹. Furthermore, visual field tests can vary for one patient in between visits due to daily form, medication and learning¹².

OCT imaging

Optical Coherence Tomography (OCT) is based on interferometry; a group of techniques aiming to superimpose waves. Superimposition occurs as two waves match in phase and frequency; they will join to form a resultant wave with an amplitude that may be greater, identical or lower than the original. The Fourier principle states that information about each component wave can be extracted from a resultant wave when they are superimposed.

Coherence as a term is used when describing properties of two separate waves with a fixed phase relationship, i.e. when their phase difference is constant. Coherency is a prerequisite to form stable interferometric patterns.

A broadband light source produces a beam of coherent waves that travels through a Michelson interferometer, which splits the waves. One wave is directed to a reference mirror and the other to the retina. At the retinal layers some light will be absorbed by the tissue and the rest scattered. Within a single tissue e.g. the retina, each layer has different refractive index and scatter accordingly. The scattered light travels back to the interferometer and meets light reflected from the reference mirror; only when their respective waves are in phase an interference signal is given to a photodetector, and a scan (an A-scan) subsequently made. As scatter wavelengths and their time delay differ depending on retinal layer depth, the reference mirror must move to adjust for variations in time of flight. More A-scans are made as the reference mirror moves. Several A-scans form a B-scan; the latter thus constitutes a 2D rendition of the retinal layer. Several B-scans can be then put together to create a 3D image.

The first generation, Time Domain (TD-) OCT, utilizes interference signals based on time delays for image capture. The dependency on moving the reference mirror to sequentially scan deeper retinal depths imparts a speed limitation.

A further evolution of the OCT, Spectral Domain (SD-) OCT, gives information about retinal depth by deconstructing the scatter and reference waves into different wavelengths as according to the Fourier principle. A broad wavelength light source is divided into a spectrum with diffraction, then it is projected to a spectroscope where interference is achieved. SD-OCT technology removes the need for adjusting the reference mirror; the efficiency of scanning all retinal depths simultaneously greatly increases the operating speed. The spectral domain OCT (SD-OCT) is thus faster than TD-OCT^{13,14} and a study conducted when SD-OCT still was relatively new, found that even without additional segmentation software SD-OCT had higher reproducibility for assessing peripapillary RNFL thickness compared to TD-OCT¹⁵.

A limitation of the SD-OCT is the requirements on the light source; a prerequisite for OCT analysis are coherent waves with short intervals and a light source producing a broad range of wavelengths in turn.

As a solution to this limitation Swept-Source (SS)-OCT was introduced, where division of the wavelengths in the light source is achieved by utilizing tuneable lasers. This increases capture speed compared to SD-OCT. SS-OCT has been used in a clinical setting since 2012¹³. Interestingly, a comparative study conducted in 2016 suggests that the SD-OCT may have a better ability than SS-OCT to detect thinning of the ganglion RGC layer in the outer temporal area of the macula¹⁶. Another study found that SS-OCT outperformed SD-OCT when measuring choroidal thickness¹⁷.

Measuring the RNFL in ONH with OCT

The layers of the retina are visualized with various signal contrast in grayscale OCT images. Ideally, the retinal pigmental epithelium will appear white due to light scattering from the granules and is distinguished as the innermost layer in the OCT image. Distinguishing RPE from Bruch's membrane is not always possible and depends on resolution potential along the sagittal axis¹⁸.

Recognizing the need to measure glaucomatous optic nerve damage more objectively than assessing C/D ratio from fundus photographs, Považay et. al. suggested a method to quantify RNFL axons in the ONH with OCT¹⁹. The proposed parameters were the minimal distance between the vitreoretinal interface and the central limit of retinal pigment epithelium, measured in B-scans and averaged along the circumference of the optic disc for 3D quantification. The measurement was termed MCB, Minimum Circumpapillary Band. Recognized as a measurement of RNFL axon tissue content at each cross-section of the optic disc, MCB was renamed to MDB, Minimal Distance

Band²⁰.

In 2012 Reis et. al suggested another parameter, measuring the shortest distance between Bruch's Membrane and the internal limiting membrane²¹. This parameter was termed BMO-MRW (Bruch's Membrane Opening – Minimum Rim Width).

Since detection of Bruch's membrane can be hindered by the resolution limitations of the OCT, Sandberg Melin et. al. presented new nomenclature for measuring the shortest distance between the central limit of the retinal pigmental epithelium (OPCL, ONH Pigment epithelium Central Limit) and the closest point of the inner limit of the retina (IRCP, Inner limit of the Retina Closest Point)²². This distance is thus termed PIMD, Pigment epithelium central limit – Inner limit of the retina Minimal Distance (Appendix 1). The average PIMD measured over the entirety of the ONH is therefore termed PIMD-2 π .

All mentioned methods have the same aim: to utilize measuring parameters for objective assessment of RNFL axon content in the ONH. A major advantage of these thickness parameters is that they are specifically designed to measure B-scans acquired from 3D sources. This removes the need of reference planes, as is necessary when measuring in 2D radial OCT scans.

Estimation with algorithms in 3D-OCT captures

During 2016 Tsikata et. al. used MDB parameters with Spectralis SD-OCT for 3D segmentation of the ONH, concluding that it had a higher diagnostical capability than older 2D RNFL measurements in specific quadrants of the neuroretinal rim²³.

Several approaches to segmentation for representation of the ONH from 3D sources have been made with both MDB and BWO-MRW parameters²³⁻²⁵, none of these automatic. An automatic algorithm has so far only been tried for 2D radial B-scans centred on the ONH²⁶. Only Spectralis (Heidelberg, Germany) OCT devices offer a software for automatic segmentation, using BWO-MRW. Regardless, this method requires manual control and correction of erroneous delineations.

For PIMD, a semi-automatic approach has been used so far²². OPCL is marked manually in every one of 500 radial slices of B-scan images under the assumption that pigment epithelium only crosses each slice once. Blood vessels can obscure RPE with shadowed, low-signal areas; instead of manual markup the semi-automatic algorithm interpolates the two closest slices that are marked to estimate the distance. IRCP is automatically identified in every image. The resulting distance PIMD

and its end points is tracked in a Cartesian coordinate system referenced from a 3D cube capture protocol.

A fully automatic algorithm used in this project is has been developed and run in a specifically designed software. The goal is proper automatic detection of both OPCL and IRCP. A machine learning algorithm which references predefined delineation samples is used for this process. Previously, Miri et. al. has tried machine learning for 3D segmentation in glaucomatous eyes using BMO-MRW and found that the A.I approach had less errors than previous non-automatic approaches²⁷.

Method

Subjects

Volunteers in the ages of 30-69 were selected according to the inclusion criteria listed in Table 1. All criteria were self-reported; if discovered with a condition hindering OT capture the participant in question would thus be excluded from the study. A full ophthalmological examination was offered to all participants with suspect disease discovered at the time of image capture. Participants were recruited in Gävle Hospital and Uppsala Akademiska Sjukhuset.

Table 1. Inclusion criteria

Variables	Criteria
Age (years)	$\geq 30, \leq 69$
Refractive error (D)	$> -5, < 5$
No family history of glaucoma	
No conditions that hinders OCT examination	

Procedure

20 minutes prior to examination subjects were administered with pupil-dilating tropicamide 5 mg/ml in both eyes. Then, subjects were seated at the OCT. Head level was adjusted to a comfortable position at the frame of the OCT. The eye not to be examined was occluded with an eyepatch. With the subject ready and in place, the chair was locked to hinder lower body movement. The head position was then

further tuned so that the corner of eye to be examined matched the frame marking. Before capture, the light in the room was turned off.

A 3D Macula cube 6×6 mm capture protocol was used first as a proper fixation target. Then, the protocol was switched to 3D Glaucoma disc cube 6×6 mm, in which the capture was made.

Between every successful capture the subject was asked to rise from the chair to reposition. The process was then repeated.

Three consecutive captures of the right eye followed by the left eye were made. Blinking and horizontal eye movement affects the quality of the captured image. Loss of visual information in the image due to blinking presents as black bands; these images were discarded and retaken. Images with visible jagged joins due to horizontal eye movement were also discarded. A total of three good quality images of each eye, six in total, were made. All captures were made with the same operator and machines using an identical procedure.

OCT imaging

Images were acquired with SD-OCT models Topcon 2000 (DRI OCT Triton, Topcon, Japan) at Gävle Hospital and SS-OCT Topcon Triton (DRI OCT Triton, Topcon, Japan) at Uppsala Akademiska Sjukhuset.

Both machines enable a 3D capture of the ONH. The 3D cube capture protocol contains visual information within predefined volumetric dimensions. These differ between OCT models (Table 2). Each scan along a plane yield a specific number of pixels. Sequential A-scans are made along the frontal plane. Several adjacent A-scans equals one B-scan. A complete cube is comprised of adjacent B-scans along different depths (Fig. 2). Within the completed volume the 3D equivalent to one pixel is a voxel.

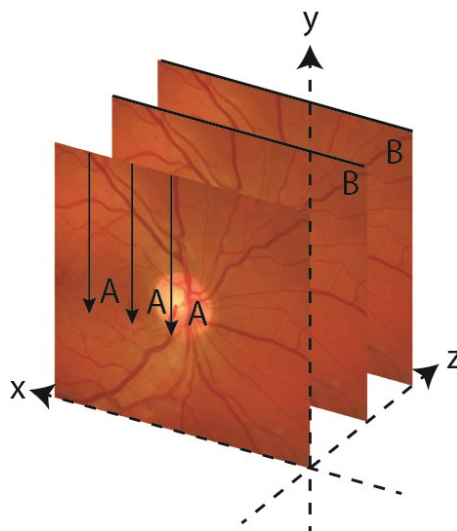


Fig 2. Schematic representation. Arrays of A-scans form B-scans. Arrays of B-scans form a cube in a three-dimensional Cartesian coordinate system.

Table 2. Specifications of Topcon 3D-OCT machines

	Frontal axis (x)	Longitudinal Axis (y)	Sagittal Axis (z)
Number of pixels (Px)			
Topcon 2000	512 Px	128 Px	885 Px
Topcon Triton	512 Px	256 Px	992 Px
Cube dimensions (mm)			
Topcon 2000	6.0 mm	6.0 mm	2.3 mm
Topcon Triton	6.0 mm	6.0 mm	2.6 mm

The 3D volumes are exported to a research computer with a custom-made program specifically designed for automatic delineation of PIMD. A frontal projection of the cube is presented in the program interface, in which the operator manually marks the center of the ONH. The cube is resampled into polar coordinates in a cartesian coordinate system, with the operator's chosen center as origin. Within the cube each voxel will represent a specific point in the coordinate system. When run, the program constructs 500 equally spaced radial slices originating from the origin point (Fig. 3). In each of these slices, detection of OPCL and IRCP to delineate PIMD is automatically performed. As with the semi-automatical segmentation, The AI starts the detection nasally and continues counter-clockwise and clockwise in the frontal plane for the right and left eye respectively. Like the semi-automatic method, blood vessels which obscure the image are not marked for OPCL.

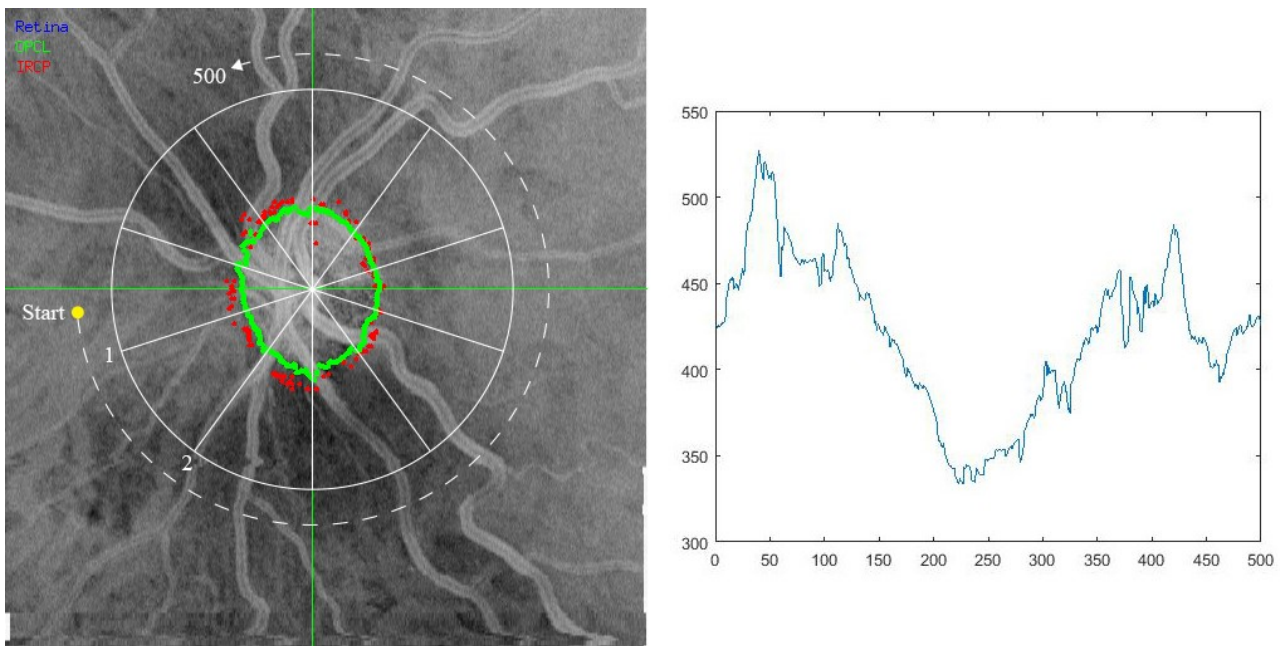


Fig 3. Left image is the schematic representation of equally spaced radian slices over the frontal projection of the 3D cube as seen in the program interface in *white*. Segmentation begins as indicated by “Start” in *yellow* and continues counter-clockwise. Right image shows the corresponding PIMD measurement (y-axis) as a function of angle (x-axis) (right). Sample from 40-year old female.

Experimental design

16 subjects were examined, evenly distributed among volumes, age groups and sex. All subjects were examined following their respective age groups in an ascending order.

Table 3. Distribution of subjects in groups and their order of examination

Groups (ages)	1. (30-39)	2. (40-49)	3. (50-59)	4. (60-69)
Examination order and subject number (Order within group)	1 (1) 5 (2) 9 (3) 13 (4)	2 (1) 6 (2) 10 (3) 14 (4)	3 (1) 7 (2) 11 (3) 15 (4)	4 (1) 8 (2) 12 (3) 16 (4)
Number of subjects				
Men	2	2	2	2
Women	2	2	2	2
Total	4	4	4	4

The mean PIMD over 500 radians, termed PIMD- 2π , is calculated for each of three volumes for one subject in one eye. It is thus the mean PIMD- 2π for one eye. The mean PIMD- 2π for each age group is calculated by averaging the PIMD- 2π values for all subjects within the group.

Statistical parameters

Due to small sample size the confidence coefficient was set to 0.95.

Analysis of variance (ANOVA) with a hierarchal mixed model was chosen for estimation of the differences in mean PIMD- 2π among volumes and subjects. All samples were balanced across groups, volumes and number of subjects within each group were equal. The independent variables were subjects and volumes. The dependent variable is PIMD- 2π .

Null hypothesis (H_0) was that all group PIMD- 2π means are equal.

Results

Captures of good quality were obtained from 16 subjects. A total of 18 subjects participated. Two subjects were excluded; one retrospectively reported first-grade family history of glaucoma, the

other due to difficulties obtaining an acceptable image quality to bilateral keratoconus. One subject in group 3 was called back one month later to retake captures of the left eye due to image artifacts interfering with proper segmentation.

For calculation of PIMD- 2π , the left eye samples presented with a higher number of quality images and thus were chosen for statistical and visual analysis. For two samples in the entire data set, a third volume value had to be averaged from two volumes to complete a full data set.

Variation of PIMD as a function of angle

In the normal eye samples of the left eye, PIMD- 2π presented with double hump pattern when PIMD was plotted against angle. The graphs of all samples were manually investigated. Within most subjects, all three volumes of the left eye presented with similar patterns, including the samples with the least similarity between the three volumes (Fig. 4). Subject 3 was the sole sample presenting without a double hump pattern.

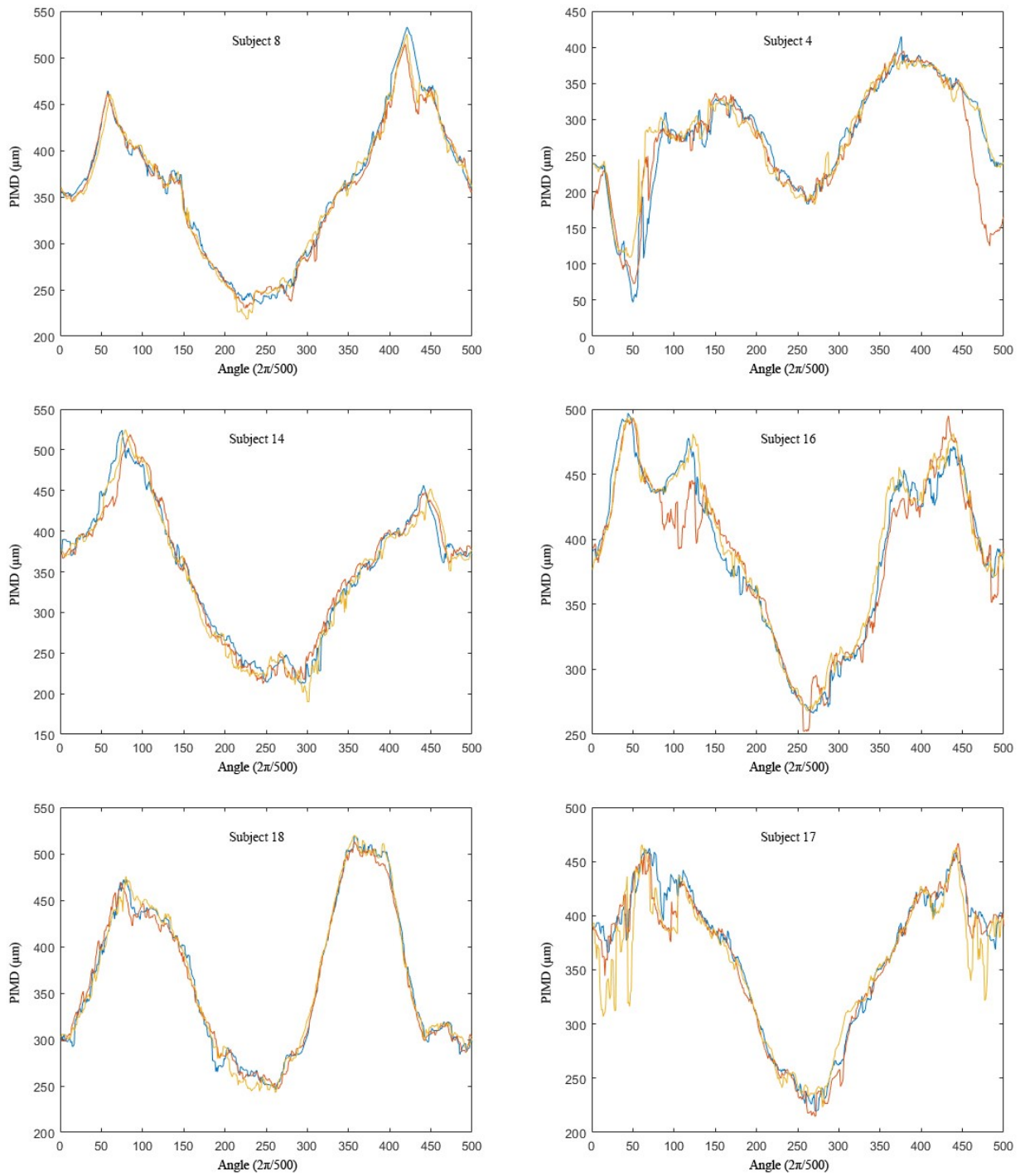


Fig. 4. Left graph column shows the three best matched segmentations for all volumes from three subjects. Each segmented PIMD pattern is indicated in yellow, red and blue. Right graph column shows the least matching segmentations. PIMD (y-axis, μm) as a function of angle (x-axis, $2\pi/500$).

ANOVA analysis

To establish the sources of variation among subjects and volumes an analysis of variance with a nested (hierarchical) mixed model was performed. The model proposes that each PIMD-2 π measurement (x_{ijk}) is a sum of the population PIMD-2 π mean (μ), the random variation among groups (A_i), subjects ($B_{j(i)}$), and volumes ($\epsilon_{k(ij)}$).

$$x_{ijk} = \mu + A_i + B_{j(i)} + \epsilon_{k(ij)} \quad \text{Eq. 1}$$

The ANOVA analysis was performed with BMDP8V (BMDP Statistical Software Inc., Los Angeles). The dependent variable was PIMD-2 π . The independent variables were subjects and volumes. The fixed variable was groups.

Table 4. Sources of variation in estimates of PIMD-2 π in non-glaucomatous eyes

Source of variation	Estimated variance (μm^2)	Degrees of freedom (d.f.)
Subjects	2758.20975	12
Volumes	7.717468	32

The analysis found that the variation among volumes was two magnitudes lower than the variation among subjects. ANOVA F-test result was 1.99 ($F_{3:12;0.95} = 4.47$). The grand mean of all PIMD values for volumes was $344.3 \pm 56.3 \mu\text{m}$. The mean PIMD-2 π for each age group is presented below (Table 5).

Table 5. Average PIMD-2 π for each age group.

Group	Age (years)	Average PIMD2-pi (μm) \pm S.D.
1	30-29	376.0 ± 33.5 (CI 95%)
2	40-49	292.3 ± 51.4 (CI 95%)
3	50-59	364.6 ± 61.6 (CI 95%)
4	60-69	344.3 ± 49.9 (CI 95%)

Normal loss rate

Plotted in a linear regression graph, the results showed a negative trend. The y-axis represents the mean PIMD- 2π of the left eye. The x-axis shows age. In the equation for the linear regression model (Fig. 5), the slope variable was -2.43, which represents a loss rate of -2.43 $\mu\text{m}/\text{year}$ in non-glaucomatous samples of one eye. The estimated loss rate in percent per year is thus 0.52% ($-2.43 \div 467.0$). The percentual loss per decade is thus 5.2%.

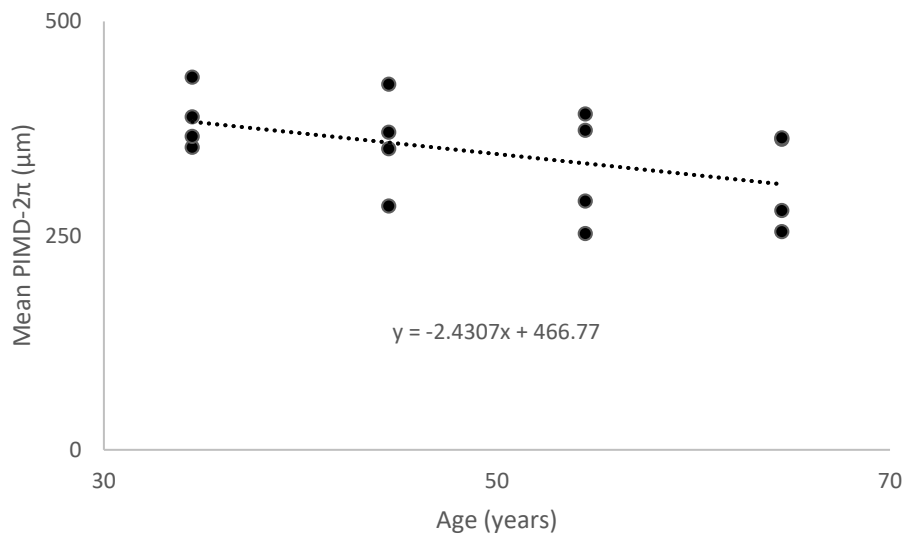


Fig. 5. Measurements from 16 subjects plotted in a scatter diagram with linear regression equation. Mean PIMD- 2π (y-axis, μm) as a function of medians of the age groups (x-axis, years).

Performance of the program

Taking the time needed to manually mark the center of the ONH into consideration, analysis of one volume takes approximately 1 minute. This time depended on image quality; images with jagged clipping through the ONH took longer time. As shown below, OPCL is marked in green and IRCP in red.

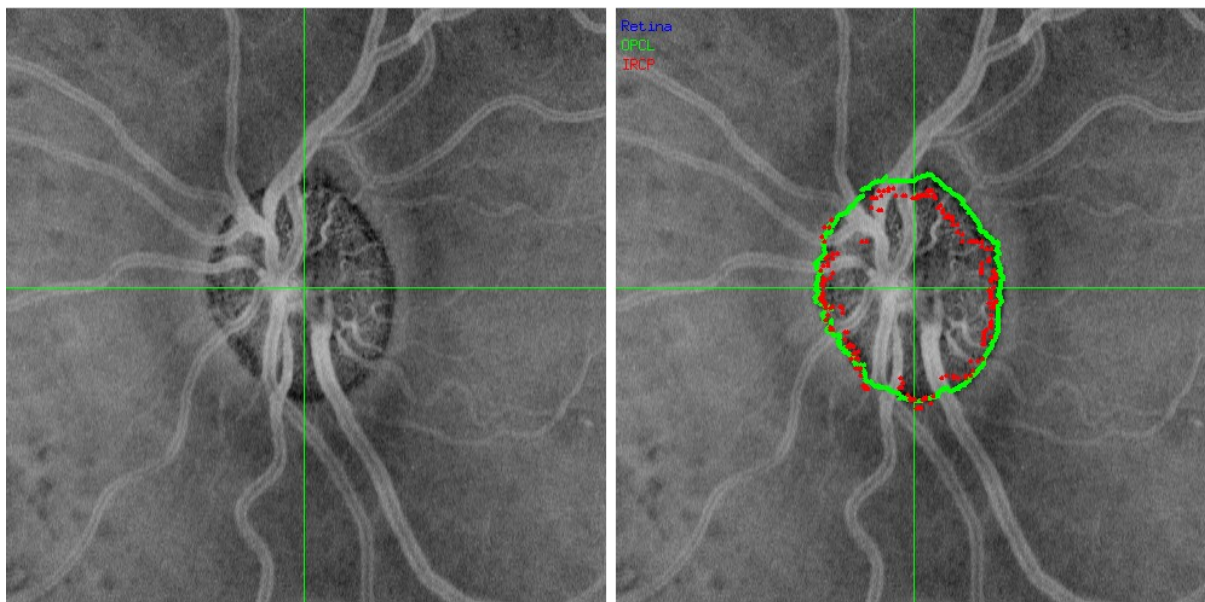


Fig. 6. Topcon Triton ONH B-scan as it appears in the program (interface cropped away). Before segmentation (left) and after (right). Sample of left eye from a 30-year old female.

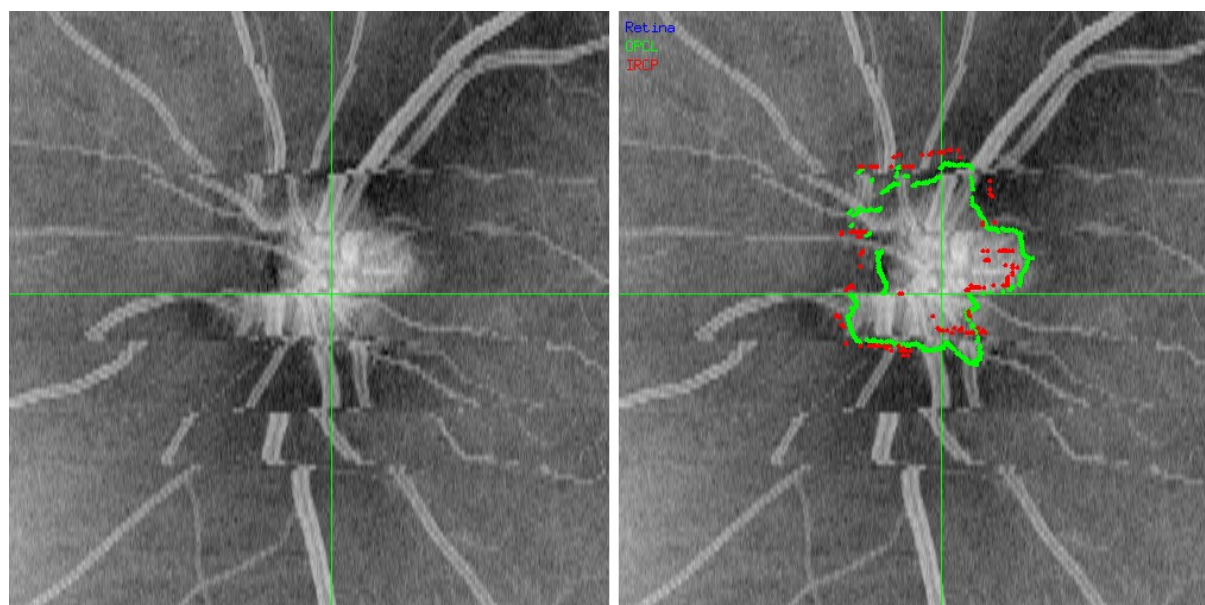


Fig. 7. Topcon 2000 ONH B-scan as it appears in the program (interface cropped out). Before segmentation (left) and after (right). This B-scan has fragmented image artefacts due to horizontal eye movement. Because of this the resulting segmentation is interrupted and non-continuous. Sample of left eye from a 30-year old male.

Discussion

Results

The ANOVA F-test results showed that there is no difference in mean PIMD- 2π between different age groups. The F-test result, 1.99, was compared to a distribution table listing critical values for the chosen statistical parameters ($F_{3:12:0.95} = 4.47$). Because the F-test result was lower than the critical value ($1.99 < 4.47$), the null hypothesis could not be rejected.

Furthermore, the sample size is small and has a large variation among subjects, which is why conclusions cannot be drawn from ANOVA analysis alone whether there is an age-related loss of NFL axons in the ONH.

The linear regression showed a negative trend. Due to the large subject variation, it remains unknown whether the trend is statistically significant or not.

The variation in mean thickness of the NFL among subjects is of large; this is confirmed in other studies of both healthy and glaucomatous eyes using 3D-OCT parameters^{24,25}. Using PIMD as a parameter, the subject variance of PIMD- 2π in 40 sampled glaucomatous eyes has been estimated to $1280 \mu\text{m}^2$ ²⁸, which is of the same magnitude order as the results in this study but a lower number. The very high variance number in this study can be explained by a comparatively smaller sample size.

The variance of PIMD- 2π within volumes in this study is of a very small magnitude. It is one magnitude than a previously measured volume variance of $30 \mu\text{m}^2$ in glaucomatous eyes²⁸. The study sampled eyes from 6 subjects; a low size which may raise the variance.

For the parameter BMO-MRW in larger samples of healthy eyes, the variability was found to be lower in a sample size of 30 subjects²⁸. Measurements were taken from one eye at one occasion by one observer. The variability result was 2.88 (2.37-3.4, CI 95%), reported as reproducibility with within-subject standard deviation. Since the standard deviation is the square root of variance, the variances in the mentioned and current study can be considered to have the same magnitude.

A previously calculated mean PIMD- 2π from 8 segmentations of one healthy eye using the semi-automatic method was $212 \pm 10 \mu\text{m}^2$. Comparing this to the mean PIMD- 2π of four subjects in the same age group, it is difficult to say what result is more accurate due to such small sample sizes.

The mean PIMD of 48 samples measured with the automatic algorithm agrees somewhat with previous data.

For MDB and BMO-MRW the global means are $307.5 \pm 41.2 \mu\text{m}^{24}$, $312 \pm 41 \mu\text{m}^{23}$ and $301.9 \pm 57.8 \mu\text{m}^{25}$ respectively. Both studies sampled non-glaucomatous eyes for measurement of the minimal NFL content in cross-sections of the ONH with a 3D cube protocol.

The difference in these measurements may be due to a wide range of size and shape differences of the ONH in the population. With a larger ONH, the RGC axons have more space to distribute around the ONH; in the frontal plane RGC axons will not be as packed and PIMD will thus be smaller.

Comparing individual PIMD- 2π measurements to a normative database for glaucoma diagnosis and follow-up is not advantageous due to the large variation in normal samples. It is more advantageous to compare samples from the same patient over time; because within-subject variability is low for both smaller and larger sample sizes. Furthermore, the estimated variance for occasions was lower than for volumes²⁸. Radical changes in mean PIMD- 2π could signal a pathological loss of RGC axons.

The estimated loss rate of $-2.43 \mu\text{m}/\text{year}$, albeit higher than expected in a non-glaucomatous eye, is in concordance with previously measured rates of change. Using BMO-MRW on 3D cube samples from 60 non-glaucomatous subjects, a mean loss rate of $-1.47 \mu\text{m}/\text{year}$ has been reported ($-2.56, -0.06, \text{CI } 95\%$)²⁵. The same study found a loss rate of $-2.37 \mu\text{m}/\text{year}$ ($-3.93, -0.76, \text{CI } 95\%$) in glaucomatous eyes. In this study, the Spectralis (Heidelberg, Germany) OCT machine was used (Heidelberg, Germany), with a higher resolution and slower speed. It is therefore impossible to generalize these results for data obtained with other OCT machines.

Method

Originally, three samples of each eye were to be included. After reviewing the B-scan image in the program interface, a substantial number of right-eye samples had to be excluded due to interrupting artefacts across the ONH. Using the mean of two measurements to construct a third is not preferred over obtaining a full set of volumes; in this case it was performed due to ANOVA analysis requiring perfectly balanced samples. For other statistical methods, such as within-subject standard deviation, balanced samples are not required. ANOVA was chosen so that all data could be processed simultaneously, which presents a significant time advantage.

PIMD as a measurement reflects the number of NFL axons in one frontal cross-section of the ONH. In this project, each PIMD measurement was averaged over the entire ONH (2π radians) in μm .

Arguably, PIMD could also be measured as an area over 2π in μm^2 , since it would still represent the number of RGC axons in a cross section²⁹. For this, a radius of the ONH would need to be estimated which can add an uncertainty factor³⁰.

For a significant amount of the samples in this study, it was not apparent until the images were opened in the program interface that there were artefacts hindering proper analysis of the ONH. This was especially for samples captured with the older SD-OCT model Topcon 2000. It was later noted that the OCT software lacked a component which helped to immediately identify an image ruined by artefacts.

Capture time needs to be faster than eye movement to optimally rid images of shifts. Topcon Triton utilises the swept-source technique whilst Topcon 2000 uses spectral domain. Topcon Triton performs 100 000 A-scans per second compared to Topcon 2000, which has half the speed (50 000 A-scans per second).

An unexperienced OCT operator may need to take more captures for each subject to ensure there will be enough adequate material. This is not always possible in the daily clinical work setting and especially for the patient, who will at some point experience eye fatigue and perform worse. Statistically, averaging more than three volumes can be considered as oversampling²⁸.

With more OCT scans and especially segmentations, the unexperienced operator will improve for each occasion. Detection of PIMD parameters may become more accurate with time. This introduces a subjective uncertainty. It is important that this type of uncertainty is diminished by a strict examination order, in which subject groups are distributed evenly according to age groups to avoid pooling of method accuracy in specific age groups. This study borrowed the method from previous semi-automatic student project studies with PIMD; when commencing this study, it was not certain the automatic algorithm would be finished in time for analysis. Using an automatic algorithm greatly reduces the risk of introducing a subjective assessment of PIMD parameters.

This study was not designed to statistically measure the performance of the automatic algorithm. However, as each volume sample was manually investigated during each segmentation, it became clear that the algorithm produced more continuous segmentations of PIMD with the faster OCT model Topcon Triton. Not surprisingly, a higher scan speed mitigates eye movement more effectively. With an experienced operator, and more examination time, there should in theory be no hindrance to

capture adequate quality images regardless of machine. At present, the image quality needs to be assessed before running the algorithm. This may introduce a subjective factor.

It was noticed that the algorithm does not always skip detection in areas where blood vessels obscure the OPCL. In several images, the algorithm detected the border of a blood vessel as the IRCP. Although a correction of this is needed in the future, the statistical impact of erroneous detection of IRCP is diminished when averaging three volumes over π .

The study aimed to include as many participants as possible with the goal of 80; Sandberg Melin et.al. estimated an optimal sample size if three volumes per subject is averaged at one occasion by one observer²⁸ by investigating sample size as a function of power. It was also found that a significant difference in mean PIMD can be detected with a sample size of 180 subjects.

There were difficulties recruiting participants in certain age groups; later in the process a reward had to be introduced in the form of a free cinema ticket to meet the sample size requirements in a limited amount of time. This introduced a potential risk of false self-reports as it could urge participants to enroll regardless of them meeting the exclusion criteria.

In the samples, two sets of four participants were closely related. Two participants as siblings, and two others as parent-child. Within small sample sizes, including siblings of similar age in the same group could potentially lead to a misrepresentation of the mean. For a larger study sample. One study involving dizygotic twins shows that morphometry of the ONH was significantly similar in both monozygotic and dizygotic twins³¹.

This project is to be expanded in the future, with recruitment of more participants 160 subjects and refinement of the automatic algorithm method. Therefore, an ethical approval was applied for and granted by the local ethics committee. All subjects were anonymized with a specific code system kept separate from their social security numbers and contact information. Signed consent was collected from all subjects. The Helsinki Declaration guidelines were followed.

Future

Currently, there are no precise longitudinal studies on NFL axon loss in healthy eyes with PIMD and other parameters. An accepted rate of change needs to be balanced with a defined pathological loss, to optimize earlier detection and less false positive diagnosis of glaucoma. To map the normal rate of

change for use in a clinical context a much larger sample size of healthy eyes needs to be used in future studies, and preferably include subjects older than 69 years, since the prevalence increases exponentially with older age³².

The automatic segmentation program needs to be adjusted and enhanced further. In preparation for a clinical setting, the program should have the capacity to accurately handle less than optimal images, even where eye shifts have resulted in discontinuous and fragmented images. A possibility would be to enable a reconstruction of fragmented images, since no actual information is lost as is the case when the patient blinks.

Conclusion

The mean PIMD- 2π did not differ in four age groups distributed over a span of 30-69 years.

Linear regression analysis presented with a trendline which suggests a non-glaucomatous age-related loss of RGC axons in the ONH with an estimated rate of $-2.43 \mu\text{m}/\text{year}$. The usage of a fast, fully automatic algorithm for delineation of PIMD produced results that are in accordance with previous, semi-automatic method findings.

Capturing than more than three volumes from each sample is not statistically necessary but may be required if the operator is inexperienced to ensure that there is enough quality material. Currently, the program running the automated algorithm is sensitive to fragmented images due to horizontal eye movement and needs to be further adjusted. The program performed better when paired with a faster OCT.

Acknowledgements

The program using an automatic algorithm to measure PIMD was designed and written by Gabriel Carrizo. The author would like to thank prof. Per Söderberg, who saw possibilities and helped me find my way with this project in my hometown. To my student project supervisor Zhaohua Yu for the practical help with in-lab analysis, statistics, patience, explanations, and constantly opening the locked lab doors when I called. Camilla Sandberg Melin for support at Gävle Hospital, as well as being enthusiastic and knowledgeable about her thesis subject. And to one participant, who will remain anonymous, volunteering to help me distribute recruitment flyers, e-mails, and generally spreading the word.

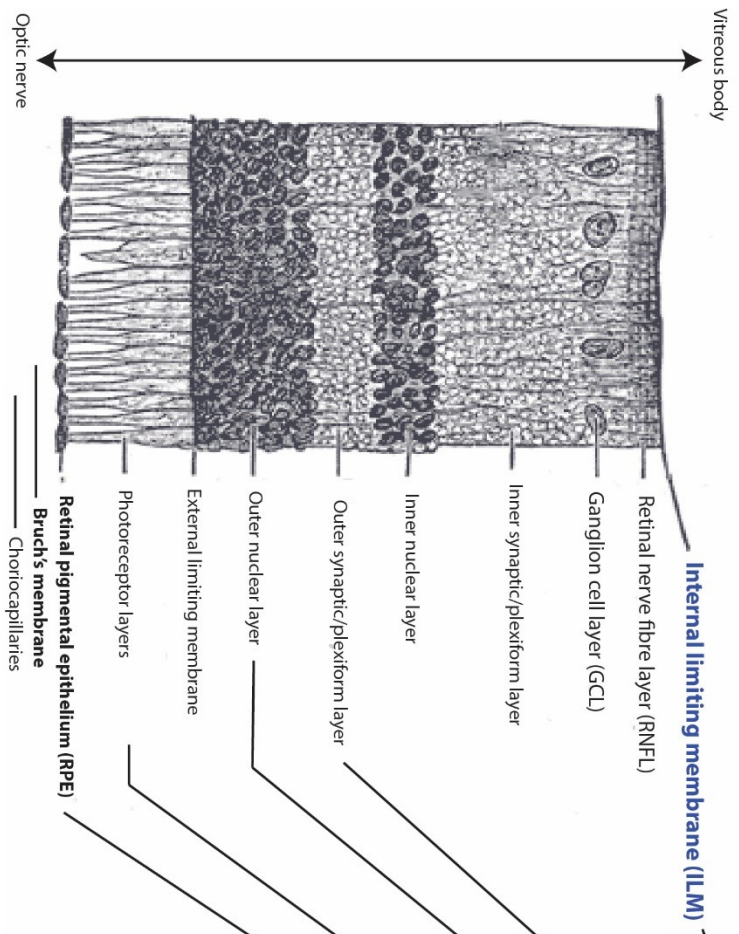
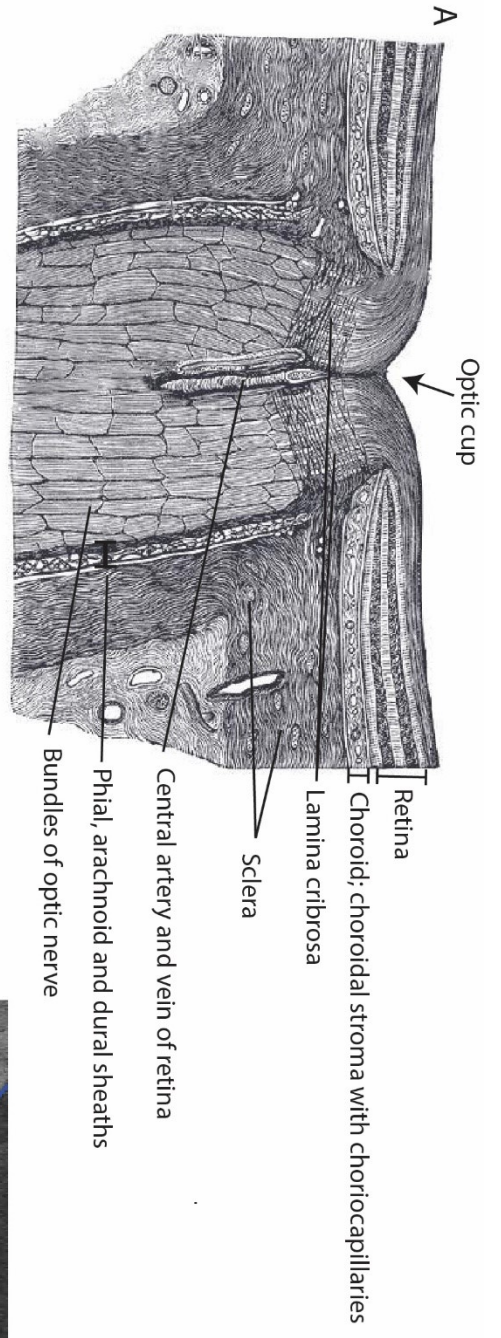
References

1. Dichtl A, Jonas JB, Naumann GOH. Retinal nerve fiber layer thickness in human eyes. *Graefe's Archive for Clinical and Experimental Ophthalmology*. 1999;237(6):474-479. doi:10.1007/s004170050264
2. Quigley HA. The Size and Shape of the Optic Disc in Normal Human Eyes. *Arch Ophthalmol*. 1990;108(1):51. doi:10.1001/archopht.1990.01070030057028
3. Kingman S. Glaucoma is second leading cause of blindness globally. *Bull World Health Organ*. 2004;82:887-888. doi:10.1590/S0042-96862004001100019
4. Quigley HA, Jampel HD. How Are Glaucoma Patients Identified? *Journal of Glaucoma*. 2003;12(6):451.
5. Agarwal R, Gupta SK, Agarwal P, Saxena R, Agrawal SS. Current concepts in the pathophysiology of glaucoma. *Indian J Ophthalmol*. 2009;57(4):257-266. doi:10.4103/0301-4738.53049
6. Calkins DJ. Critical pathogenic events underlying progression of neurodegeneration in glaucoma. *Progress in Retinal and Eye Research*. 2012;31(6):702-719. doi:10.1016/j.preteyeres.2012.07.001
7. Yorio T, Krishnamoorthy R, Prasanna G. Endothelin: Is It a Contributor to Glaucoma Pathophysiology?: *Journal of Glaucoma*. 2002;11(3):259-270. doi:10.1097/00061198-200206000-00016
8. Weinreb RN, Aung T, Medeiros FA. The Pathophysiology and Treatment of Glaucoma: A Review. *JAMA*. 2014;311(18):1901-1911. doi:10.1001/jama.2014.3192
9. Sommer A, Katz J, Quigley HA, et al. Clinically Detectable Nerve Fiber Atrophy Precedes the Onset of Glaucomatous Field Loss. *Arch Ophthalmol*. 1991;109(1):77-83. doi:10.1001/archopht.1991.01080010079037
10. Hattenhauer MG, Johnson DH, Ing HH, et al. The probability of blindness from open-angle glaucoma. *Ophthalmology*. 1998;105(11):2099-2104. doi:10.1016/S0161-6420(98)91133-2
11. Sheldrick JH, Ng C, Austin DJ, Rosenthal AR. An analysis of referral routes and diagnostic accuracy in cases of suspected glaucoma. *Ophthalmic Epidemiology*. 1994;1(1):31-39. doi:10.3109/09286589409071443
12. Hutchings N, Wild JM, Hussey MK, Flanagan JG, Trope GE. The Long-Term Fluctuation of the Visual Field in Stable Glaucoma. *Invest Ophthalmol Vis Sci*. 2000;41(11):3429-3436.
13. Kishi S. Impact of swept source optical coherence tomography on ophthalmology. *Taiwan Journal of Ophthalmology*. 2016;6(2):58-68. doi:10.1016/j.tjo.2015.09.002

14. Forte R, Cennamo GL, Finelli ML, Crecchio G de. Comparison of time domain Stratus OCT and spectral domain SLO/OCT for assessment of macular thickness and volume. *Eye*. 2009;23(11):2071-2078. doi:10.1038/eye.2008.363
15. Schuman JS. Spectral Domain Optical Coherence Tomography for Glaucoma (An AOS Thesis). *Trans Am Ophthalmol Soc*. 2008;106:426-458.
16. Lee KM, Lee EJ, Kim T-W, Kim H. Comparison of the Abilities of SD-OCT and SS-OCT in Evaluating the Thickness of the Macular Inner Retinal Layer for Glaucoma Diagnosis. *PLOS ONE*. 2016;11(1):e0147964. doi:10.1371/journal.pone.0147964
17. Copete S, Flores-Moreno I, Montero JA, Duker JS, Ruiz-Moreno JM. Direct comparison of spectral-domain and swept-source OCT in the measurement of choroidal thickness in normal eyes. *British Journal of Ophthalmology*. 2014;98(3):334-338. doi:10.1136/bjophthalmol-2013-303904
18. Drexler W, Fujimoto J. State-of-the-art retinal optical coherence tomography. *Progress in Retinal and Eye Research*. 2008;27(1):45-88. doi:10.1016/j.preteyeres.2007.07.005
19. Považay B, Hofer B, Hermann BM, et al. Minimum distance mapping using three-dimensional optical coherence tomography for glaucoma diagnosis. *JBO*. 2007;12(4):041204. doi:10.1117/1.2773736
20. Chen TC. Spectral domain optical coherence tomography in glaucoma: qualitative and quantitative analysis of the optic nerve head and retinal nerve fiber layer (an AOS thesis). *Trans Am Ophthalmol Soc*. 2009;107:254-281.
21. Reis ASC, O'Leary N, Yang H, et al. Influence of clinically invisible, but optical coherence tomography detected, optic disc margin anatomy on neuroretinal rim evaluation. *Invest Ophthalmol Vis Sci*. 2012;53(4):1852-1860. doi:10.1167/iovs.11-9309
22. Sandberg Melin C, Malmberg F, Söderberg PG. A strategy for OCT estimation of the optic nerve head pigment epithelium central limit-inner limit of the retina minimal distance, PIMD- 2π . *Acta Ophthalmol*. 2019;97(2):208-213. doi:10.1111/aos.13908
23. Tsikata E, Lee R, Shieh E, et al. Comprehensive Three-Dimensional Analysis of the Neuroretinal Rim in Glaucoma Using High-Density Spectral-Domain Optical Coherence Tomography Volume Scans. *Invest Ophthalmol Vis Sci*. 2016;57(13):5498-5508. doi:10.1167/iovs.16-19802
24. Shieh E, Lee R, Que C, et al. Diagnostic Performance of a Novel Three-Dimensional Neuroretinal Rim Parameter for Glaucoma Using High-Density Volume Scans. *American Journal of Ophthalmology*. 2016;169:168-178. doi:10.1016/j.ajo.2016.06.028
25. Kabbara SW, Zangwill LM, Munda R, et al. Comparing optical coherence tomography radial and cube scan patterns for measuring Bruch's membrane opening minimum rim width

- (BMO-MRW) in glaucoma and healthy eyes: cross-sectional and longitudinal analysis. *Br J Ophthalmol*. 2018;102(3):344-351. doi:10.1136/bjophthalmol-2016-310111
26. Belghith A, Bowd C, Weinreb RN, Zangwill LM. A hierarchical framework for estimating neuroretinal rim area using 3D spectral domain optical coherence tomography (SD-OCT) optic nerve head (ONH) images of healthy and glaucoma eyes. In: *2014 36th Annual International Conference of the IEEE Engineering in Medicine and Biology Society*. Chicago, IL: IEEE; 2014:3869-3872. doi:10.1109/EMBC.2014.6944468
27. Miri MS, Abramoff MD, Kwon YH, Sonka M, Garvin MK. A Machine-Learning Graph-Based Approach for 3D Segmentation of Bruch's Membrane Opening from Glaucomatous SD-OCT Volumes. *Med Image Anal*. 2017;39:206-217. doi:10.1016/j.media.2017.04.007
28. Melin C, Yu Z, Söderberg P. Variance components for PIMD- 2π estimation of the optic nerve head and consequences in clinical measurements of glaucoma. *Acta Ophthalmologica*. July 2019. doi:10.1111/aos.14197
29. Gardiner SK, Ren R, Yang H, Fortune B, Burgoyne CF, Demirel S. A method to estimate the amount of neuroretinal rim tissue in glaucoma: comparison with current methods for measuring rim area. *Am J Ophthalmol*. 2014;157(3):540-549.e1-2. doi:10.1016/j.ajo.2013.11.007
30. Sandberg Melin C. Morphometry of the Optic Nerve Head as a Diagnostic Tool for Glaucoma. 2019. <http://urn.kb.se/resolve?urn=urn:nbn:se:uu:diva-393989>. Accessed January 6, 2020.
31. Tang L, Scheetz TE, Mackey DA, et al. Automated Quantification of Inherited Phenotypes from Color Images: A Twin Study of the Variability of Optic Nerve Head Shape. *Invest Ophthalmol Vis Sci*. 2010;51(11):5870-5877. doi:10.1167/iovs.10-5527
32. Tham Y-C, Li X, Wong TY, Quigley HA, Aung T, Cheng C-Y. Global Prevalence of Glaucoma and Projections of Glaucoma Burden through 2040. *Ophthalmology*. 2014;121(11):2081-2090. doi:10.1016/j.ophtha.2014.05.013

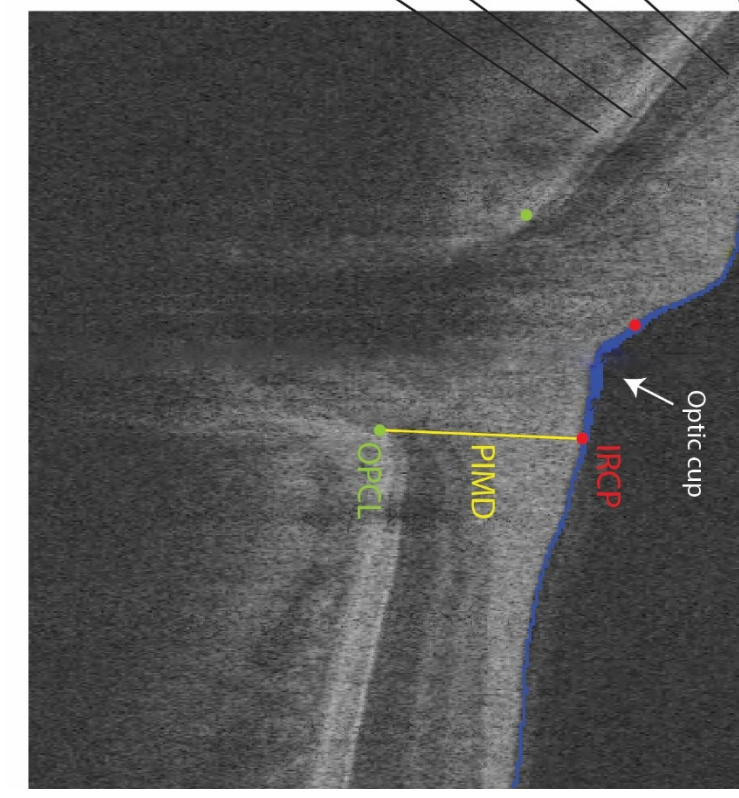
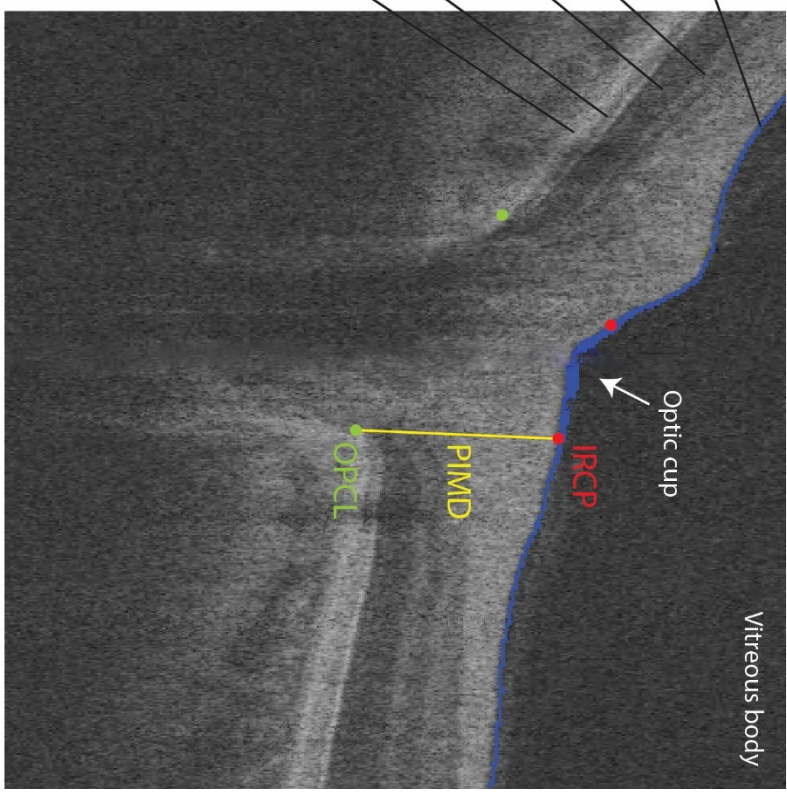
Appendix 1 Anatomy of the ONH and its appearance in an OCT B-scan



B

Internal limiting membrane (ILM)

C



A: Illustration of the optic nerve head, ONH. (Reworked from Gray's Anatomy, 1918)

B: Illustration of the retinal layers. (Reworked from Gray's Anatomy, 1918).

C: Frontal projection of the 3D cube as it appears in the automatic algorithm software. The parameters have been drawn for visualisation purposes; they appear differently in the software UI.